nature communications

Article

https://doi.org/10.1038/s41467-024-52174-z

Structural basis of Frizzled 4 in recognition of Dishevelled 2 unveils mechanism of WNT signaling activation

Received: 24 February 2024

Accepted: 28 August 2024

Published online: 02 September 2024

Check for updates

Yu Qian[1,6], Zhengxiong Ma[1,6], Zhenmei Xu[1], Yaning Duan[1], Yangjie Xiong[1], Ruixue Xia[1], Xinyan Zhu[1], Zongwei Zhang[2], Xinyu Tian[2], Han Yin[1], Jian Liu[1], Jing Song[1], Yang Lu[1], Anqi Zhang[2], Changyou Guo[2], Lihua Jin[3], Woo Jae Kim[1], Jiyuan Ke[4], Fei Xu[5], Zhiwei Huang[2] & Yuanzheng He[1]

WNT signaling is fundamental in development and homeostasis, but how the Frizzled receptors (FZDs) propagate signaling remains enigmatic. Here, we present the cryo-EM structure of FZD4 engaged with the DEP domain of Dishevelled 2 (DVL2), a key WNT transducer. We uncover a distinct binding mode where the DEP finger-loop inserts into the FZD4 cavity to form a hydrophobic interface. FZD4 intracellular loop 2 (ICL2) additionally anchors the complex through polar contacts. Mutagenesis validates the structural observations. The DEP interface is highly conserved in FZDs, indicating a universal mechanism by which FZDs engage with DVLs. We further reveal that DEP mimics G-protein/β-arrestin/GRK to recognize an active conformation of receptor, expanding current GPCR engagement models. Finally, we identify a distinct FZD4 dimerization interface. Our findings delineate the molecular determinants governing FZD/DVL assembly and propagation of WNT signaling, providing long-sought answers underlying WNT signal transduction.

WNT signaling is a highly conserved and intricate molecular pathway that plays a pivotal role in numerous biological processes, including embryonic development, tissue regeneration, and disease pathogenesis[1–3]. Dysregulation of WNT signaling is associated with various diseases, including cancer, osteoporosis and degenerative illnesses, making it a crucial area of intense biomedical research. The signaling is initiated by the simultaneous engagement of WNT ligand to the extracellular cysteine-rich domain (CRD) of a Frizzled receptor (FZD) and to an extracellular domain (ECD) of the co-receptor LRP5 or LRP6[4,5]. In canonical WNT signaling, the active WNT-FZD-LRP5/6 complex recruits the key transducer protein, Dishevelled (DVL), to the plasma membrane (PM) of cells, which then serves as a hub to recruit Axin, and in turn to bring glycogen synthase kinase-3 β (GSK3β) and casein kinase 1 (CK1) to PM to form the membrane associated signalosome (Supplementary Fig. 1a). Formation of the signalosome triggers the collapse of the destruction complex (DC) which leads to the stabilization and nuclear translocation of β-catenin, where it collaborates with T cell factor/lymphoid enhancer-binding factor (TCF/LEF) to orchestrate the transcription of WNT target genes[6]. There are also two β-catenin independent non-canonical WNT signaling pathways, the planar cell polarity (PCP) pathway and the Ca^{2+} pathway[7] which are less characterized than the canonical pathway.

FZDs belong to the class F G-protein coupled receptor (GPCR) subfamily which encompasses 10 FZDs (FZD1-10) and a smoothened receptor (SMO)[8]. All FZDs contain a conserved CRD, followed by a flexible linker before the transmembrane domain. While FZDs primarily interact with DVL and initiate WNT signaling, specific members of the FZD family can also engage with G-proteins[9–11]. Additionally,

[1]Laboratory of Receptor Structure and Signaling, HIT Center for Life Sciences, School of Life Science and Technology, Harbin Institute of Technology, Harbin, China. [2]School of Life Science and Technology, Harbin Institute of Technology, Harbin, China. [3]Northeast Forestry University, Harbin, China. [4]Institute of Health and Medicine, Hefei Comprehensive National Science Center, Hefei, China. [5]iHuman Institute, ShanghaiTech University, Shanghai, China. [6]These authors contributed equally: Yu Qian, Zhengxiong Ma. e-mail: ajian.he@hit.edu.cn

although all FZDs can bind to WNT, it's important to note that FZD4 is the only receptor known to recognize Norrin[12], an atypical WNT ligand. Furthermore, there is evidence to suggest that FZDs have the capacity to form homodimers in both WNT-dependent and WNT-independent manners[13,14]. Notably, Norrin has a nature of being dimerized through covalent bonds, and each monomer is capable of binding to one CRD of the dimeric FZD4[15,16]. However, it has also been demonstrated that monomeric FZDs are able to activate WNT signaling alone[17], which leaves the functional significance of dimerized FZDs shrouded in mystery.

DVLs play an essential role in mediating WNT signaling by bridging the connection between the receptor and downstream proteins[18]. They act akin to G-proteins by directly interacting with the active receptor and relaying the signal to downstream effectors. There are three DVLs (DVL1-3) in human, each consisting of three conserved domains, namely DIX, PDZ, and DEP, arranged sequentially from the N-terminal to the C-terminal region, interconnected by intrinsically disordered linkers. The DIX domain is responsible for DVL polymerization and DVL-Axin1 interaction. The PDZ domain has been shown to interact with a highly conserved KTxxxW motif of the helix 8 (H8) of FZDs in vitro[19,20]. However, whether this interaction occurs in cells and its role in signalosome assembly are not clear. In contrast, the DEP (Dishevelled, Egl-10, and Pleckstrin) domain has emerged as the primary driver of the interaction between FZD and DVL[21]. The DEP domain of DVL is a compact domain consisting of approximately 100 amino acid residues, comprising a three-helix bundle, a β-hairpin 'arm' (finger-loop) and two short β-strands at the C-terminal region (C-loop)[22]. It has been observed that DVL can autonomously associate with FZD without WNT[23], however, the interaction is markedly enhanced upon adding of WNT ligand. Interestingly, a recent study shows FZD-DVL interaction is positively regulated by the lipid $PI(4,5)P_2$[24]. The latest research showed that WNT stimulation dynamically regulate the FZD-DVL interaction, and the extracellular agonist cooperates with the intracellular transducer to maintain the complex in active conformation for downstream effector recruitment, a reminiscent of the classical GPCR activation[23]. Furthermore, DVL2 has been shown to undergo liquid-liquid phase separation that is crucial for controlling the assembly of the Wnt receptor signalosome[25]. DVL has also been shown to localize in nucleus and affect gene transcription, moreover, to promote cancer cell invasion, migration and proliferation[26].

The advances in structural studies make substantial contributions to our comprehension of WNT signal transduction. For instance, the crystal structure of Xenopus WNT8 (XWNT8) in complex with the CRD of mouse Fzd8 revealed the ligand recognition model of FZD[27], and the CRD-truncated apo FZD4 structure unveiled the architecture of the transmembrane domain of FZD4[28]. Despite the structural progresses on illuminating each component of the WNT/FZD/LRP signaling complex, two fundamental questions still remain: first, how the ligand binding signal is transferred to the transmembrane domain to activate the receptor; second, how the receptor passes the activation signal to the key transducer, DVL, to initiate downstream signaling cascade (Supplementary Fig. 1a).

To unravel the central enigma of WNT signaling, we solved the cryo-EM structure of FZD4 bound with the DEP domain of DVL2. Given the pivotal role of the DEP domain of DVL in mediating the FZD/DVL interaction, we designate DEP as the DEP domain of DVL thereafter, unless otherwise specified. Our structural analysis has unveiled a distinct engagement model of FZD4/DEP, which stands in stark contrast to the canonical GPCR/G-protein engagement model. Additionally, we have revealed the active conformation of FZD4 for DEP recognition, as well as a, to the best of our knowledge, previously undiscovered dimerization interface of FZD4. The insights gleaned from our study lay the foundational groundwork for understanding WNT signaling.

Results

FZD/DVL interaction is mainly mediated by the DEP domain of DVL

We chose FZD4 and DVL2 as the model for investigating FZD/DVL interaction due to the sole ability of FZD4 to interact with both WNT and Norrin ligands[12] and the fact that DVL2 is the most extensively studied DVL protein. Our initial exploration aimed to determine whether the DEP domain serves as the primary mediator of the FZD4-DVL2 interaction. To assess the domain contributions to FZD interaction, we employed three DVL2 constructs: the full-length DVL2, the PDZ-DEP construct in which the DIX domain and the flexible C-terminus region have been omitted, and the DEP domain alone (Fig. 1a). In the TOPFlash assay, a gold-standard assay for the measurement of WNT signaling activation, both WNT3a and Norrin induce an increase of reporter activity without exogenous transfection of DVL2 protein (the first column of Fig. 1b, c), indicating WNT3a and Norrin activate FZD4

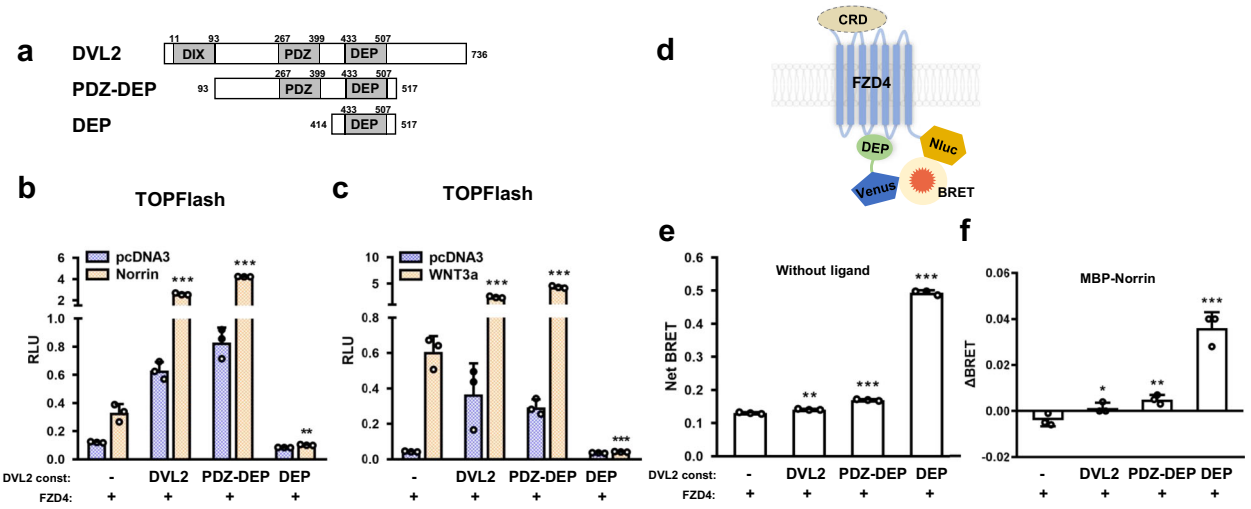

Fig. 1 | The relay of WNT signaling is mainly mediated by the DEP domain of Dishevelled. a A schematic diagram of the DVL2 constructs used in this study. **b**, **c** The TOPFlash assay for Norrin (**b**) or WNT3a (**c**) stimulated FZD4 activity. Data are presented as mean values ± SD; $n = 3$ independent samples; Two-side T-test. See source data for each exact p value. RLU: relative luciferase unit. **d** A schematic diagram of the BRET assay used for detecting FZD/DVL interaction. **e, f** BRET assay of FZD4/DVL2 interaction, **e** for basal activity and **f** for MBP-Norrin (10 μg/ml) induced activity. Data are presented as mean values ± SD; $n = 3$ independent samples; n.s. no significant; *$p < 0.05$; **$p < 0.01$; ***$p < 0.001$; Two-side T-test. See source data for each exact p value. Source data are provided as a Source Data file.

through endogenous DVLs in the AD293 cells. The induction is diminished without FZD4 transfection, indicating that the activation is indeed mediated through FZD4 (Supplementary Fig. 3a). The exogenous transfection of full-length DVL2 significantly boosts both the basal and ligand induction activity (The second column of Fig. 1b, c). Interestingly, the exogenous transfection of the PDZ-DEP domain exhibits a stronger induction activity than the full-length DVL2 (the 3rd lane of Fig. 1b, c), consistent with the observation that the DIX domain has an inhibitory effect on DVL2, and the combination of PDZ and DEP (PDZ-DEP) domain is sufficient to initiate complete WNT signaling[23]. Western-blot shows that the increase of receptor activity by the PDZ-DEP construct is not attributed to higher expression level compared to full-length DVL2 (Supplementary Fig. 1b). To our surprise, the exogenous transfection of DEP almost totally abrogates ligand induced FZD4 activity (the last column of Fig. 1b, c, compared with the 1st column). We reasoned that the exogenously transfected DEP competes with the endogenous DVLs for FZD4 binding. Since DEP binding of the receptor alone is not able to recruit downstream effectors, the competitive binding of DEP with the endogenous DVLs results in a squashing of receptor activity, a dominant negative effect that has been seen for many receptors[29–31]. To validate this hypothesis, we used DVL1/2/3 triple knock-out (TKO) HEK293T cells[25] to repeat the WNT3a/Norrin induction assays. In the DVL1/2/3 TKO HEK293T cells, there is no WNT3a/Norrin induction without the exogenous transfection of DVL2, and the dominant negative effect of DEP disappears due to the absence of endogenous DVLs to compete with (Supplementary Fig. 3b), suggesting that WNT indeed signals through DVL, with DEP being the primary binding domain for DVL to engage with FZD.

A similar activity of DEP is also observed in FZD5 (Supplementary Fig. 1c). These findings underscore the pivotal role of the DEP domain in the interaction between FZD and DVL. We also used a bioluminescence resonance energy transfer (BRET) assay, where FZD4 is fused with Nluc and DVL2 is fused with Venus, to assess the domain contribution of DVL2 in the interaction with FZD4 (Fig. 1d). In the absence of ligand, the full-length DVL2 only marginally increases the basal BRET signal while the PDZ-DEP construct shows a moderate increase of basal BRET signal (Fig. 1e). Conversely, the DEP construct causes a strong increase of the basal BRET signal, demonstrating that the FZD4/DVL2 interaction is predominantly mediated by the DEP domain. Similarly, when the ligand Norrin (MBP-Norrin) is added to the system, the DEP domain exhibits a robust increase of BRET signal, whereas the PZD-DEP domain and full-length DVL2 only slightly increase the signal (Fig. 1f). It is noteworthy that the BRET assay and TOPFlash assay provide distinct perspectives: the BRET assay measures the interaction between the receptor and DVL, whereas the TOPFlash assay assesses the outcome of signaling.

The overall structure of FZD4/DEP complex

The FZD-DVL interaction has been notoriously difficult to investigate for several reasons. First, DVL dynamically switches from monomer to oligomer due to the DIX-DIX interaction. Second, the FZD/DVL interaction is disrupted upon cell lysis. Third, the large flexible region between each domain of DVL hindered the structural determination of FZD/DVL complex. Our initial attempt of obtaining full-length receptor in complex with full-length DVL failed due to the high instability of the CRD domain of FZD4 and the weak interaction between the receptor and the full-length DVL2. We then decided to obtain a CRD-truncated receptor in complex with DEP, the core domain for receptor interaction. In class A GPCR, it has been shown that receptor on the PM constantly switches between active and inactive conformation, forming a transient complex with the transducer (e.g. Gα protein) without ligand stimulation, a phenomenon known as receptor "breathing"[32,33]. The complex can be stabilized by either ligand binding or increasing local concentration of the binding partners. For this reason, we adopted the NanoBiT technology[34] where the C-terminus of the CRD-truncated FZD4 was fused with the large part of NanoBiT (LgBiT) and the C-terminus of DEP was fused with the renovated high affinity peptide of NanoBiT (HiBiT) (Supplementary Fig. 1d and details see Methods). The NanoBiT tethering strategy has been successfully used in solving multiple GPCR/G-protein complexes structures, particularly those complexes with weak or dynamic associations[35–39]. Based on the ligand and transducer cooperation theory, we hypothesized that a substantial increase in the local concentration of binding partners could promote the formation of a receptor/transducer complex under conditions of very low or even "zero" ligand concentration. Indeed, the NanoBiT tethering strategy enabled apo 5HT1A to complex with G_i in an active conformation identical to ligand-bound 5HT1A[40]. Similar phenomenon has also been seen in the bitter taste receptor TAS2R46, where the G-protein engaging model of apo TAS2R46 is identical to that of strychnine-bound TAS2R46[38].

Based on above observations, we co-expressed the CRD-truncated human FZD4 fused with LgBiT and the DEP fused with HiBiT in *Spodoptera frugiperda* (Sf9) cells and purified the complex. The purification profile indicates that FZD4 forms complexes with DEP in both monomeric and dimeric configurations, with distinct peaks for each configuration (Supplementary Fig. 1e and details see Methods). Due to the small size of the monomeric complex (< 60 kDa) and the absence of a distinct fiducial marker, we were unable to attain a sufficiently high-resolution structure of the monomer (Supplementary Fig. 1g). In contrast, the dimeric complex displayed significantly improved features in the 2D classification, allowing us to solve the complex at 3.43 Å to reveal the engagement details of the complex (Supplementary Figs. 1f, 2a, b and Supplementary Table 1).

The dimer is mainly formed by two FZD4 transmembrane domains. Protomer A (ProtA) exhibits a better density than protomer B (ProtB) (Fig. 2). While the trace amount of density on the protomer B cytoplasmic side suggested that DEP is also able to associated with ProtB (Supplementary Fig. 1f left lower panel) but the complex is much weaker, explaining why we were only able to solve one DEP in the complex. Further local refinement on ProtA improves the resolution to 3.35 Å (Fig. 2 and Supplementary Fig. 2a). The extracellular side of FZD4 is not well resolved due to the flexibility of the region and the small size of the complex. Nevertheless, the transmembrane domain and the interface between FZD4 and DEP are well resolved, enabling us to obtain structural insight into DEP engagement of FZD4. Overall, DEP uses its finger-loop to engage the intracellular side of FZD4, a reminiscent of the G-protein engagement of class A GPCRs. It's worth highlighting that a cluster of cholesterol molecules facilitates dimerization by engaging in hydrophobic interactions with the transmembrane domain of each protomer (Fig. 2). A comparison of ProtA with ProtB shows that FZD4s of the two protomers are very similar with a root mean square deviation (r.m.s.d.) of 0.879 Å over 300 pairs of Cα (Supplementary Fig. 7b).

The FZD4/DEP engagement

Since the local refinement of ProtA shows a better density, we used it to build an atomic model for FZD4/DEP interaction. The FZD4/DEP engagement is mainly mediated by two patches of interactions. The first patch of interactions (Interface I) are the hydrophobic interactions between the transmembrane helix 5-intracellular loop 3-transmemembrane helix 6 (TM5-ICL3-TM6) of FZD4 and the finger-loop of the DEP (β1-β2); the second patch of interactions (Interface II) involve the engagement between the ICL2 of FZD4 and the groove situated between the finger-loop and C-loop of DEP (Supplementary Fig. 4a). The total buried interface is 750 $Å^2$.

On interface I, hydrophobic residues $L413^{5.69}$, $I416^{5.72}$, $L420^{5.76}$, $L430^{ICL3}$ and $L433^{6.29}$ (superscripts refer to the Ballesteros-Weinstein numbering[41]) of TM5-ICL3-TM6 of FZD4 make a close contact with the hydrophobic surface formed by $W444^{DEP}$, $L445^{DEP}$, $I447^{DEP}$ of the finger-loop of DEP (the superscript of DEP indicates residue of DEP)

https://doi.org/10.1038/s41467-024-52174-z

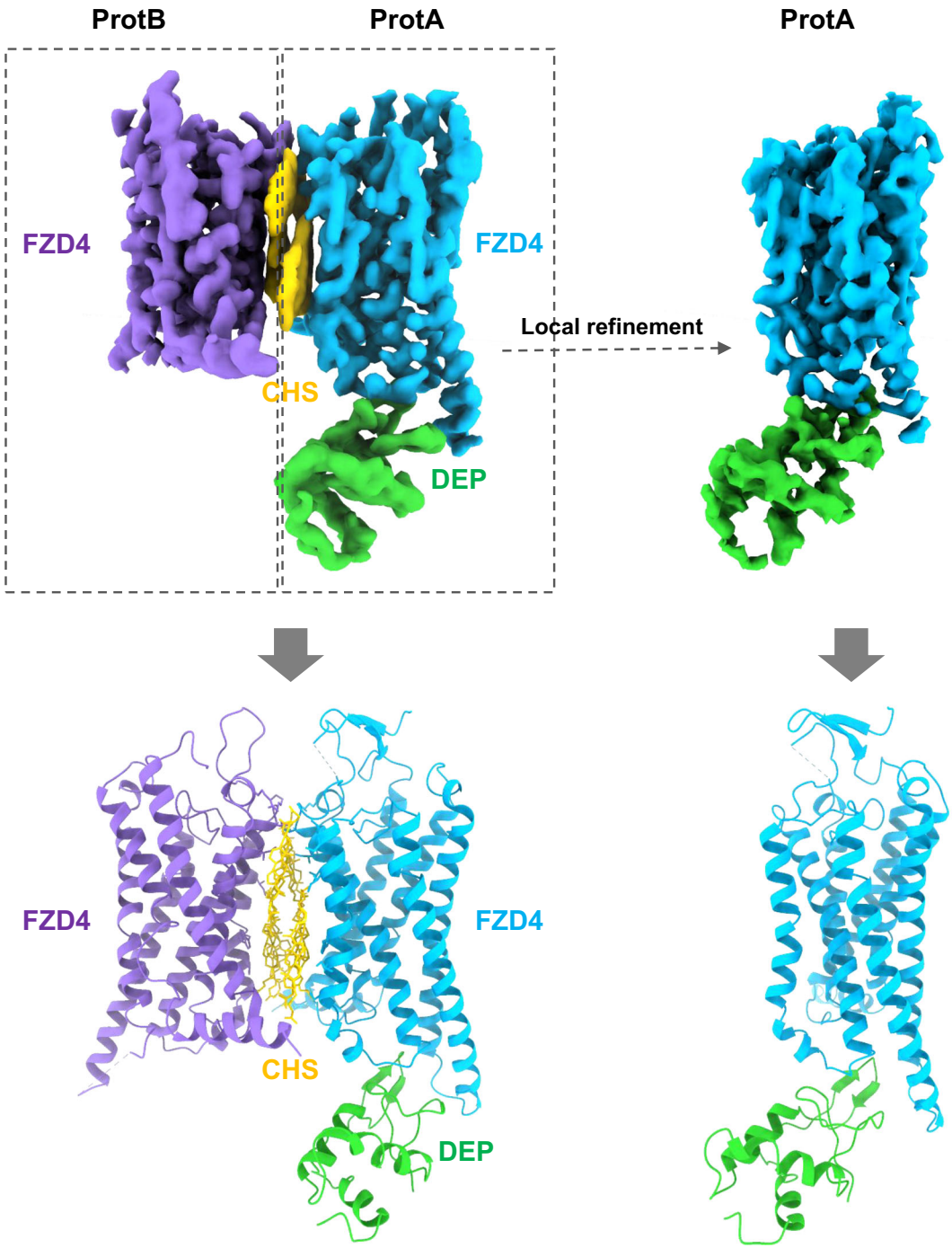

Fig. 2 | The overall structures of FZD4/DEP complexes. Upper panel, orthogonal views of the cryo-EM density map; lower panel, model of the complex in the same view and color scheme as shown in the left panel. The protomer A (ProtA) of the dimer was further local refined to generate the enhanced map of ProtA (upper right panel).

(Fig. 3a, b). Of note, K446^{DEP} is at the border of the interface; the long side chain of K446^{DEP} may also contribute to the hydrophobic interaction with the receptor. On interface II, the ICL2 of FZD is embedded into a groove formed by the finger-loop and C-loop of DEP through key polar interactions. Specifically, the backbone carbonyl group of W335^{ICL2} forms a hydrogen-bond with W444^{DEP} of the finger loop, and E338$^{4.36}$ forms polar interactions with Y502^{DEP} of the C-loop (Fig. 3c, d). In addition, R442^{DEP} is in close proximity to E338$^{4.36}$. A sequence alignment in the class F GPCR family shows that key residues on TM5-ICl3-TM6 and ICL2 that form crucial interactions with DEP are highly conserved in the FZD1-10, but not in SMO, implying that the Frizzled family employs a similar mechanism to interact with DVL (Fig. 3i). Likewise, residues on DEP that establish essential interactions with FZD4 are highly conserved among DVL1-3 (Fig. 3j).

We employed functional assays to validate the structural observation of FZD4/DEP engagement. In the TOPFlash assay, mutants of I416A$^{5.72}$, L420A$^{5.76}$, L430A^{ICL3}, L433A$^{6.29}$, W335A^{ICL2} and E338A$^{4.36}$, substantially decrease both basal activity and ligand (Norrin and WNT3a) induced activity (Fig. 3e for Norrin, Supplementary Fig. 4b for WNT3a; protein expression level, Supplementary Fig. 3c), confirming the crucial roles of TM5-ICL3-TM6 and ICL2 in DEP engagement. To rule out the influence of endogenous DVLs on the mutagenesis data, we applied these FZD4 mutants in the DVL1/2/3 TKO HEK293T cells (Supplementary Fig. 5a, b). Similarly, these mutants substantially

https://doi.org/10.1038/s41467-024-52174-z

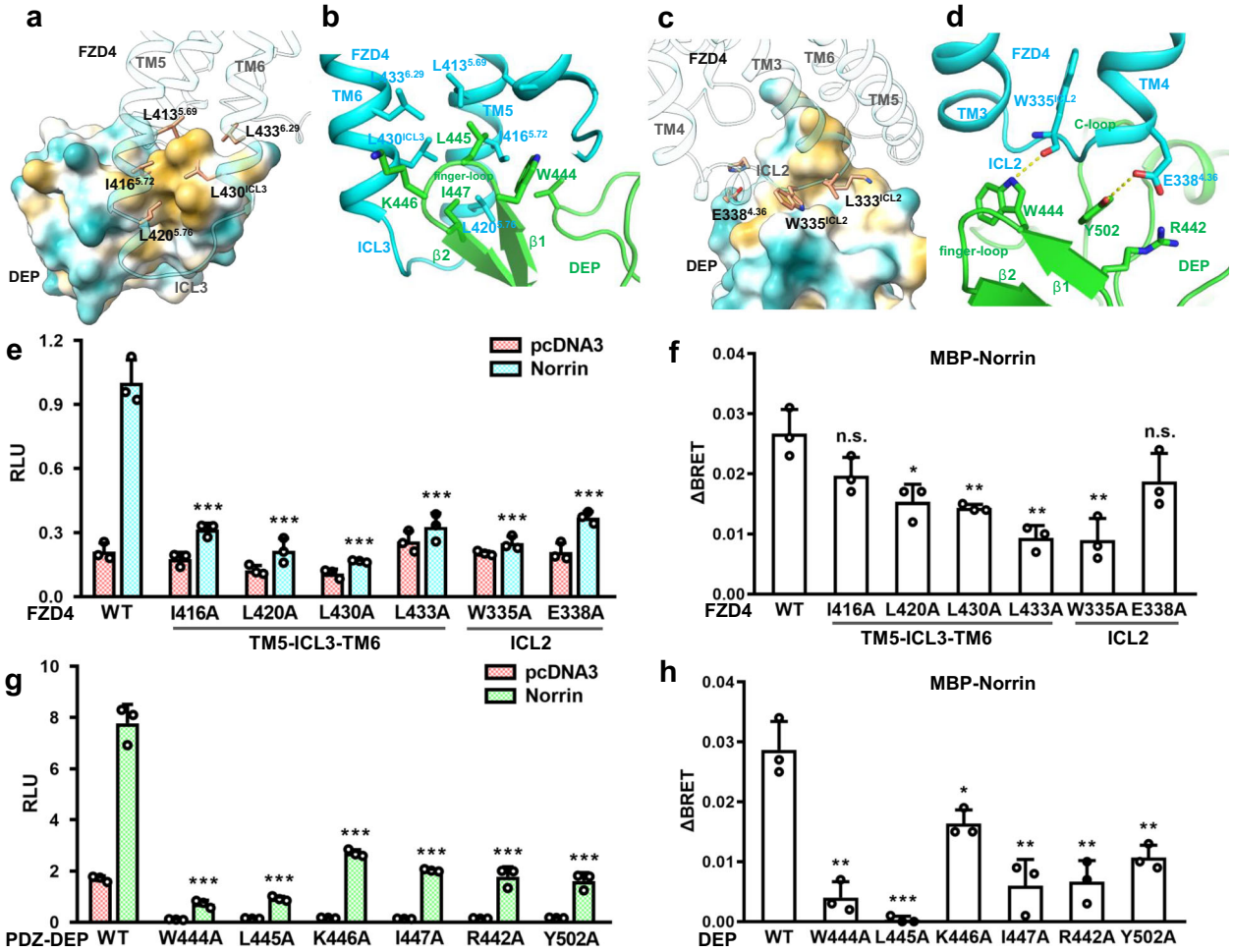

i

FZD4	ICL2		TM5-ICL3-TM6			
	W335^{ICL2}	E338$^{4.36}$	I416$^{5.72}$	L420$^{5.76}$	L430^{ICL3}	L433$^{6.29}$
FZD1	W	E	I	M	L	L
FZD2	W	E	I	M	L	L
FZD3	W	E	V	I	L	F
FZD4	W	E	I	L	L	L
FZD5	W	E	I	I	L	L
FZD6	W	E	V	I	L	F
FZD7	W	E	I	M	L	L
FZD8	W	E	I	I	L	L
FZD9	W	E	I	M	L	L
FZD10	W	E	I	M	L	L
SMO	T	Q	I	H	I	T

j

DVL2	finger loop					
	442	444	446	445	447	502
DVL1	R	W	K	L	I	Y
DVL2	R	W	K	L	I	Y
DVL3	R	W	K	L	I	Y

Fig. 3 | The FZD/DEP engagement. a A view of the TM5-ICL3-TM6 of FZD4 on the hydrophobic surface of DEP. **b** The details of the hydrophobic interactions between the TM5-ICL3-TM6 of FZD4 and the finger-loop of DEP. **c** A view of the embedding of ICL2 on the surface of DEP. **d** The details of the polar interactions between ICL2 and DEP. **e** The TOPFlash assay for FZD4 mutants w/wo Norrin. **f** The BRET assay for FZD4 mutants with the stimulation of MBP-Norrin (10 μg/ml). **g** The TOPFlash assay for DEP mutants on the context of PDZ-DEP w/wo Norrin. **h** The BRET assay for DEP mutants with the stimulation of MBP-norrin (10 μg/ml). From (**e**) to (**h**) data are presented as mean values ± SD; n.s. no significant; *$p < 0.05$; **$p < 0.01$; ***$p < 0.001$; $n = 3$ independent samples; Two-side T-test. See source data for each exact p value. Source data are provided as a Source Data file. **i** A sequence alignment of key residues for FZD4/DEP interaction in the class F GPCR family. **j** A sequence alignment of key residues for FZD4/DEP interaction in DVLs.

decrease WNT3a/Norrin-induced activity on FZD4 in the TOPFlash assay. In the BRET assay, mutants of L420A$^{5.76}$, L430A^{ICL3}, L433A$^{6.29}$, and W335A^{ICL2} largely decrease MBP-Norrin induced FZD/DEP interaction (Fig. 3f). On the DEP side, mutants of W444A^{DEP}, L445A^{DEP}, K446A^{DEP}, I447A^{DEP}, R442A^{DEP} and Y502A^{DEP} on the context of PDZ-DEP all substantially decrease both the basal and ligand induced activity in the TOPFlash assay (Fig. 3g for Norrin, Supplementary Fig. 4c for WNT3a; protein expression level, Supplementary Fig. 3c), demonstrating the essential role of the finger-loop and the groove of finger/C-loop in receptor engagement. We also observed similar results in the DVL1/2/3 TKO HEK293T cells (Supplementary Fig. 5c, d). When applying these DEP mutants on the context of DEP itself, these mutants lose their ability to compete with endogenous DVLs (Supplementary Fig. 4d, e), results in restored Norrin/WNT induction activity to the level of

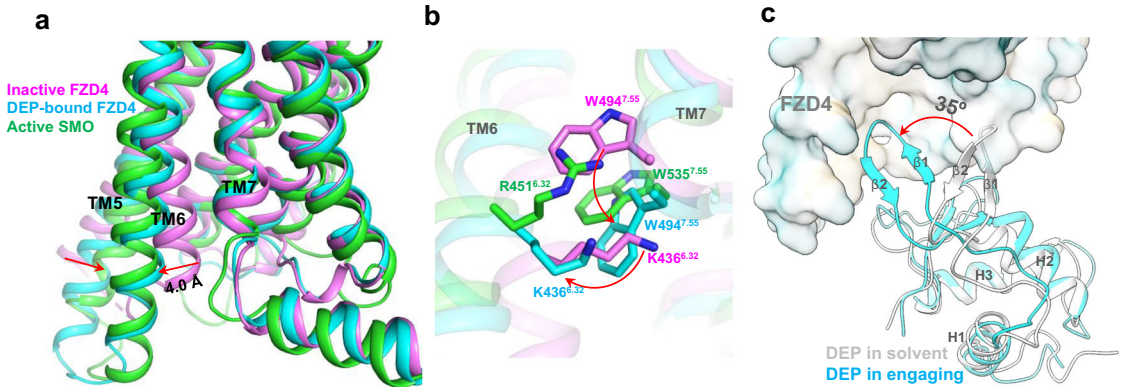

Fig. 4 | The active conformation of FZD4 and DEP. a A comparison of the overall structures of the inactive FZD4 (PDB: 6bd4), DEP-bound FZD4 and active SMO (PDB: 6ot0). **b** A comparison of the conformation change of the micro switch between the inactive receptor and active receptors. **c** A comparison of DEP conformation in solvent (PDB: 1fsh) and its conformation in engaging FZD4.

without DEP transfection (the loss of dominant negative effect), consistent with the data on the context of PDZ-DEP. In the BRET assay, these DEP mutants substantially reduce Norrin-induced FZD4/DEP interaction (Fig. 3h).

We also use DVL membrane recruitment assay to further validate our discovery. Firstly, we used a NanoBiT recruitment assay to quantify the membrane recruitment of DVL. In this assay, the C-terminus of the large part of NanoBiT (LgBiT) is fused to the CAAX membrane anchor, while the small part of NanoBiT (SmBiT) is fused to the C-terminus of DVL2 (Supplementary Fig. 6a). We then assessed the membrane recruitment of DVL2 by overexpressing FZD4 and its key DEP interface mutants. The data shows that the DEP interface mutants of FZD4 significantly decrease DVL2 recruitment to the membrane (Supplementary Fig. 6b), consistent with the FZD4 mutant data in the TOPFlash reporter assay (Fig. 3e). Secondly, we directly visualized the DVL membrane recruitment via FZD4 overexpression. In this setting, we fused FZD4 with RFP at its C-terminus and DVL2 with GFP at its C-terminus, and then co-expressed them in HeLa cells. The data shows that DVL2 was recruited to the plasma membrane by co-expression of WT FZD4, with clear colocalization on the plasma membrane (Supplementary Fig. 6c, left panel). In contrast, when co-expressed with the representative DEP interface mutant of FZD4 (I416A), DVL2 was evenly distributed in the cytoplasm, and the plasma membrane was solely occupied by the red fluorescence of FZD4, with no colocalization of DVL2 (Supplementary Fig. 6c, right panel).

To assess the conservation of the DEP interface in FZDs, we introduced mutations to key interface residues in FZD5 and examined their impact on WNT3a-induced reporter activity. The data shows that mutants of residues on TM5-ICL3-TM6 (I429A$^{5.72}$, I433A$^{5.76}$, L443A^{ICL3}, L446A$^{6.29}$) and ICL2 (W348A^{ICL2}, E351A$^{4.36}$) that form key interactions with DEP, markedly reduce reporter activity in the TOPFlash assay (Supplementary Fig. 4f; protein expression level, Supplementary Fig. 3c). Similarly, mutants of residues on DEP that establish crucial interactions with the receptor largely lose their ability to compete with endogenous DVLs to bring down FZD5 induction (Supplementary Fig. 4g; protein expression level, Supplementary Fig. 3c), implying a general mechanism by which DVLs interact with FZDs.

WNT signaling is a highly conserved pathway that regulates embryonic development from insect to mammal. We asked whether the FZD/DEP interaction mode is conserved in other species. We searched the Drosophila database and found that the DEP mutants R413H and K417M of Drosophila *disheveled (dsh)* exhibit the *dsh*^{A3} and *dsh*^{1} phenotypes, characterized by aberrant orientation of bristles and hairs[42]. The Drosophila *dsh* R413 and K417 residues correspond to human DVL2 residues R442 and K446, respectively, which are key residues of the finger loop that play a crucial role in FZD4 interaction (Fig. 3b, c). These data strongly suggest that the FZD/DEP binding mode is conserved from flies to humans.

Active conformations of FZD4 and DEP

Two pivotal questions regarding the FZD4/DEP engagement are as: Does DEP require an active conformation of the receptor for engagement, similar to the GPCR/G-protein engagement? Additionally, does DEP itself need to assume an active conformation for receptor engagement? One hallmark of GPCR activation is the outward movement of the intracellular part of TM6[43], which allows the transducer (G-protein) to engage receptor. We compared the DEP-bound FZD4 with the crystal structure of apo (inactive) FZD4[28] and noted an outward movement of TM6 (4.0 Å, measured form the Cα atom of L433$^{6.29}$), which opens up the intracellular cavity for DEP to engage the receptor (Fig. 4a). Interestingly, we also observed an inward movement of TM5 upon DEP binding. A superimposition of the active SMO (G_i coupled)[44] with the DEP-bound FZD4 shows similar conformation of TM6 and TM5, suggesting that the DEP-bound FZD4 exhibits an active conformation. We also compared the DEP-bound FZD4 with the active conformation of the G_s-coupled β2AR[43], G_i-coupled BLT1[36], G_q-coupled H1R[35] and G_{13}-coupled GPR110[45]. The comparison shows that the active FZD4 has the smallest outward movement of TM6 (4 Å) (Supplementary Fig. 7a). This observation is consistent with recent reports indicating that Class F receptors have minimal TM6 outward movement upon receptor activation[44,46]. A comparison of the protomer A with the protomer B of the FZD4 dimer shows that protomer B adopts an intermediate conformation between active and inactive receptor (Supplementary Fig. 7b), explaining why we only obtained one stable DEP within the complex.

In class A GPCRs, receptor activation is generally mediated by the cooperation of multiple conserved motif such as PIF, CWxP, NPxxY and DRY, which are notably absent in class F receptors[10,47]. A micro switch (R/K$^{6.32}$-W$^{7.55}$) has been discovered to play a crucial role in regulating class F receptor activation[10]. In the inactive state, the R/K$^{6.32}$ forms a cation-π interaction with W$^{7.55}$ to lock receptor in the inactive form; upon receptor activation, the cation-π interaction is broken. Although in the crystal structure of inactive FZD4, we did not observe a cation-π stacking interaction, we do see a coordinated movement of K436$^{6.32}$ and W494$^{7.55}$ upon receptor activation, where W494$^{7.55}$ is pushing down and K436$^{6.32}$ is displaced toward outside of TM6, similar to the conformation of active SMO (Fig. 4b). Mutants of the molecular switch in FZD4 substantially decrease ligand induction activity in both the TOPFlash and BRET assays (Supplementary Fig. 7c–e). Similar

https://doi.org/10.1038/s41467-024-52174-z

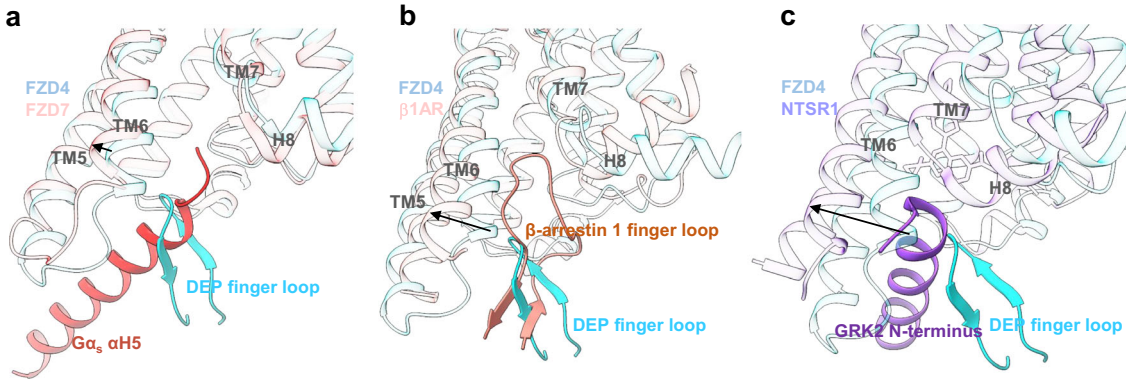

Fig. 5 | DEP vs G-protein, β-arrestin and GRK2 engagements. a A comparison the DEP engagement of FZD4 with the G_s engagement of FZD7 (PDB: 7evw). **b** A comparison of the DEP engagement of FZD4 with the β-arrestin 1 engagement of β1AR (PDB: 6tko). **c** A comparison of the DEP engagement of FZD4 with the GRK2 engagement of NTSR1 (PDB: 8jpb).

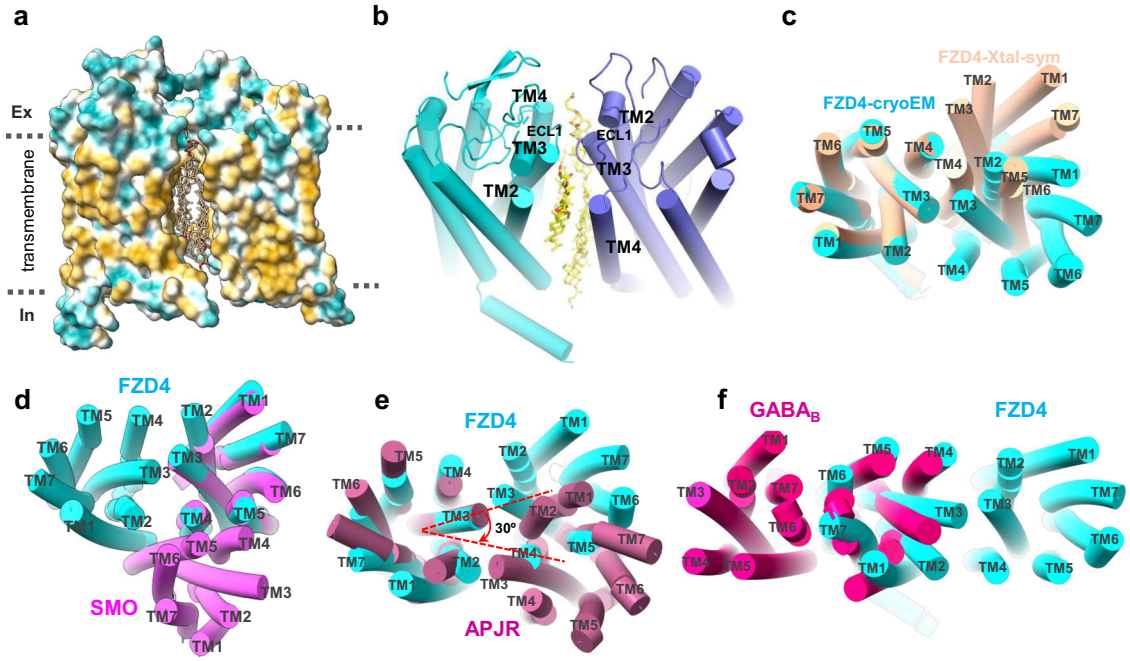

Fig. 6 | FZD4 dimerization interface. a A hydrophobic surface analysis of the FZD4 dimer. **b** FZD4 uses its TM2, TM3 and TM4 as primary interface to form the dimer. **c**–**f** Comparisons of the FZD4 cryo-EM dimer with the FZD4 crystal symmetry dimer (PDB: 6bd4), SMO dimer (PDB: 4jkv), APJR dimer (PDB: 7w0l) and $GABA_B$ dimer (PDB: 6w2y).

results are also obtained in the DVL1/2/3 TKO HEK293T cells (Supplementary Fig. 5e, f).

On the DEP side, the most striking change is the movement of finger loop (β1-β2) toward the receptor (Fig. 4c). In the NMR structure of DEP[22] within a solvent environment (inactive state), the finger-loop is oriented in an upward direction. However, upon receptor interaction, the finger-loop undergoes a 35° rotation toward the intracellular cavity of the receptor, suggesting DEP endures a substantial global rearrangement when engaging with the receptor.

DEP engagement vs G-protein, β-arrestin and GRK engagements

In canonical GPCR signaling, ligand activation of receptor induces G-protein coupling, then the activated receptor is phosphorylated by GPCR kinase (GRK) and the phosphorylated receptor is subsequently recognized and bound by β-arrestin. We therefore compared the engagement of DEP with the engagements of three major transducers (G-protein, β-arrestin and GRKs) for GPCR. We compared the DEP engagement of FZD4 with the recently reported G_s engagement of FZD7[46]. The primary distinction between DEP and G_s engagements lies in the deeper insertion of α-helix 5 (αH5) into the receptor's intracellular cavity compared to the finger-loop of DEP (Fig. 5a). Nonetheless, the total interface of the FZD7/$G\alpha_s$ is smaller than that of FZD4/DEP (630 $Å^2$ vs 750 $Å^2$) due to the additional interaction of FZD4 ICL2 with the finger-loop/C-loop of DEP (interface II, Fig. 3c, d). This difference may also account for why DVL serves as the primary partner of FZD. Of note, the classical GPCR/G-protein interface, for example the β2AR/G_s, is much bigger (1276 Å) than the FZD7/G_s engagement due to the extensive outward expansion of TM6[43]. A closer examination of the FZD7/G_s engagement reveals that the surface of αH5 is primarily hydrophilic, and the binding of αH5 to FZD7 are driven by both hydrophilic and hydrophobic interactions (Supplementary Fig. 8a, b), in contrast to the dominantly hydrophobic interaction between the

finger-loop of DEP and FZD4. When comparing the β-arrestin 1 engagement of β1AR[48] with the DEP engagement of FZD4, there is a much wider expansion of TM6 in β1AR which allows the much deeper insertion of β-arrestin 1 finger-loop than that of DEP finger-loop in FZD4 (Fig. 5b), accounting for the much bigger interface than that of FZD4/DEP (2200 Å^2 vs 750 Å^2). Both finger-loop/receptor interactions exhibit a hydrophobic nature (Supplementary Fig. 8c). The recently resolved NTSR1/GRK2 complex structure greatly expanded our understanding of GPCR signaling[49], we therefore compared the GRK2 engagement of NTSR1 with the DEP engagement of FZD4. Like the canonical GPCR activation, there is an extensively outward expansion of TM6 in the active NTSR1, allowing the N-terminal helix (αN) of GRK2 to insert deeper into the intracellular cavity of the receptor than that of the finger-loop of DEP (Fig. 5c). However, the interface of NTSR1/GRK2 is almost the same size as that of FZD4/DEP (693 Å^2 vs 750 Å^2) due the additional interaction of ICL2 of FZD4 for DEP as mentioned earlier. Similar to the finger-loop interaction, the binding of GRK2 αN to NTSR1 has a nature of hydrophobic interaction (Supplementary Fig. 8d). Taken together, the DEP engagement represents a distinct class of transducer engagement for GPCRs. A detailed comparison of the above four major transducer engagements is summarized in Supplementary Table 2.

The dimerization interface of FZD4

FZDs have been documented in monomeric, dimeric and oligomeric states under varying conditions[13,14]. The dimerization interface of FZD4 is established by the hydrophobic interactions between the transmembrane domain of each protomer and the polar interactions within the extracellular region of each protomer (Fig. 6a). Notably, the dimer interface primarily includes TM2, TM3, TM4, and the corresponding ECL1 region of each subunit (Fig. 6b). The interface has some similarity with the dimer interface seen in the crystal structure of FZD4[28] via symmetry expansion, where TM3 and TM4 are the main drivers of the dimer interface. However, the involvement of TM2 in the formation of dimer is only seen in the cryo-EM structure (Fig. 6c). When comparing the FZD4 dimer to the SMO dimer of the crystal structure[50], the key distinction lies in the fact that FZD4 dimerizes at the interface of TM2, TM3, and TM4, whereas SMO dimerizes primarily at TM4 and TM5 (Fig. 6d). Additionally, it's worth noting that in the SMO dimerization, TM4 and TM5 make direct contact with the counterpart of the other subunit. Interestingly, the FZD4 dimer is very similar to the recently reported apelin receptor (APJR) dimer[51]. Both of them are mainly driven by the hydrophobic interactions of TM2, TM3, differing only in a clockwise 30° rotation of the interface along the axle of two protomers (Fig. 6e). In the contrast, the dimer interface of the $GABA_B$ receptor[52] of class C GPCR is mainly driven by the interaction of TM6, TM7 of each subunit (Fig. 6f).

We looked at the details of the FZD4 dimer. On the extracellular side, T300$^{3.23}$ of protomer B is in close contact with K298^{ECL1} of protomer A (Supplementary Fig. 8e). On the transmembrane side, TM2, TM3 and TM4 of each promote do not directly contact, instead, a cluster of cholesterols fills in the highly hydrophobic interface of TM3, TM4 and TM5. Of note, W352$^{4.50}$ makes close contact with the hydrophobic sterol ring of the cholesterol, while H348$^{4.46}$ contacts the polar head of the cholesterol (Supplementary Fig. 8f). However, mutants of most of these residues did not yield discernible effects on receptor activity in the TOPFlash assay (Supplementary Fig. 8g, h), except a combination of K298A and T300A exhibits a marginal effect on Norrin induction in the TOPFlash assay.

Discussion

A fundamental query in WNT signaling pertains to the recruitment of DVL, the pivotal transducer, to FZD. Addressing this query has proven to be a formidable task owing to the dynamic and weak interaction between DVL and FZD. We tackled this challenge via the NanoBiT strategy through increasing local concentration of the binding partners. Indeed, this strategy has been proven to be successful in assembling complex with weak association. It's important to highlight that the NanoBiT tethering approach can enhance the affinity of dynamic or weakly associated complexes, but cannot forge an interaction that does not naturally occur. For example, we tried to establish an interaction between S1PR1 and DEP via the NanoBiT strategy, but our efforts were unsuccessful. We further validated our structural observations of the FZD4/DEP interaction via extensive functional assays, including both TOPFlash and BRET assays, affirming that our structural insights faithfully depict the authentic interaction between FZD4 and DEP.

To our surprise, DEP engages the dimeric receptor in the form of monomer, not in the form of dimer through the domain swapping model proposed in the crystal structure of DEP[53]. Unexpected, only one protomer of the FZD dimer exhibits a fully activated conformation (Supplementary Fig. 7b)., It is common in GPCR dimers for only one protomer to be active while the other remains inactive, such as in APJR[51] and as the metabotropic glutamate receptor mGlu2[54]. One reason for this phenomenon is the clash of two transducers. When we tried to docked DEP into protomer B, we noticed very close contact between two DEP (Supplementary Fig. 8i). Given that the structure reveals only part of DEP (with the N- and C-termini missing from the map) and considering the dynamic interaction between FZD4 and DEP, there is a high chance of a clash if both protomers are coupled with DEP. This may explain why only one DEP engagement was captured by the cryo-EM analysis.

Despite the well-documented presence of dimeric or oligomeric FZD receptors[14], the precise function of FZD dimerization remains an enigma within the field. In our research, we observed the existence of both dimeric and monomeric FZD4/DEP complex in our purification profile. Intriguingly, most mutations made on the dimerization interface of FZD4 did not yield any noticeable effects on receptor activity except a marginal effect of the double mutant K298A/T300A on Norrin induction. Previous study of the APJR shows that both dimer and monomer are about equally functional[51]. The physiological function of FZD dimerization is influenced by many factors, such as local concentration, membrane environment, co-receptor binding and ligand stimulation. It is important to point out that the CRD domain plays a key role in FZD4 dimerization. In case of WNT3a activation, the dimerization is not needed, whereas for Norrin activation, the dimerization of CRDs is essential[13,15,16]. The CRD domain may cooperate with the linker region connecting the CRD domain and the transmembrane domain to reinforce the dimerization. Overall, the functional importance of dimerization may hinge on the collaboration between the CRD and the transmembrane domain of FZD4.

Our structural findings, highlighting the finger-loop of DEP as the primary interface to engage the intracellular cavity of the receptor, also provides a comprehensive explanation for why previously reported mutants[13,21,23], like K446M, L445E of DEP, and L430A, L433A of FZD4, cause substantial impairment on the WNT signaling. The involvement of ICL2 to DEP interaction is out of our expectation as prior literature had indicated the TM5-ICL3-TM6 regions is the primary interface for DVL interaction[13,55]. Strikingly, residues W335^{ICL2} and E338$^{4.36}$ of the ICL2 play an essential role in complex formation by establishing vital polar interactions with key residues within the finger-loop and the C-loop (Fig. 3c, d). Notably, the key residues within TM5-ICL3-TM6 and ICL2 that mediate the DEP interaction are highly conserved across the Frizzled receptor family, but not in SMO (Fig. 3i). This observation elucidates why DVL selectively interacts with FZDs and not with SMO, even though they both belong to the same class F family of GPCRs.

Comparing to the well-established G-protein and β-arrestin engagement, as well as the established GRK engagement of GPCR, the DEP engagement of FZD represents a distinct class of engagement

of GPCR. The interface of DEP to FZD4 is much smaller than that of the G-protein and β-arrestin to classic GPCRs, but is comparable to the size of GRK2/NTSR1 interface (Supplementary Table 2). These observations align with the dynamic nature of the FZD/DVL interaction and explain the complexity of WNT signaling.

In summary, we have successfully determined the cryo-EM structure of the FZD4/DEP complex, unveiling additional structural insights into the interaction between DEP and FZD4. The insights gleaned from our study serve as a foundational resource for advancing our understanding of WNT signaling.

Methods

Constructs

For protein expression, the human Frizzled 4 gene (residues 178–537) was engineered with four specific mutations (M309L, C450I, C507F, S508Y, as previously described[28]) and inserted into the HA-tagged pFastBac plasmid. It was then fused with the LgBiT, followed by a Tobacco etch virus (TEV) cleavage site and 2xMBP. The HiBiT was attached to the C-terminus of the human DEP domain (residues 433-507), following the approach used in the VIP1R paper[34]. For TOPFlash assay, the human full length wild type Frizzled 4 gene (residues 1–537) was fused with eYFP at the C-terminus and inserted into pcDNA3. Additionally, separate pcDNA3 plasmids were utilized for inserting the human DEP domain (residues 433-507), PDZ-DEP domain (residues 93-507), and DVL2 domain (residues 1-736). For BRET assay, the human full-length wild type Frizzled4 gene was fused with Nluc at its C-terminus and inserted into pcDNA3. The cp173Venus was fused to the N-terminus of the human DVL2 constructs (full-length, PDZ-DEP, or DEP), according to the published paper[23].

Protein expression and purification

As previously mentioned[37], Spodoptera frugiperda (Sf9) cells were cultured at a density of 2×10^6 cells per ml. They were co-infected with baculovirus containing the Frizzled4-LgBiT-TEV-2MBP and the DEP protein at a ratio of 1:100 (virus volume to cell volume). After 48 h, the cells were harvested and resuspended in a buffer containing 20 mM Hepes, 150 mM NaCl, 10 mM $MgCl_2$, 20 mM KCl, 5 mM $CaCl_2$, pH 7.5, with the addition of 0.5 mU/ml apyrase. The cell suspension was then homogenized by douncing approximately 30 times. Subsequently, the mixture was incubated for 1 h at room temperature. Following the 1-h incubation, 0.5% (w/v) lauryl maltose neopentylglycol (LMNG, Anatrace) and 0.1% (w/v) cholesteryl hemisuccinate TRIS salt (CHS) were added at 4 °C and incubated for 2 h. The sample was then subjected to ultracentrifugation at 60,000 g at 4 °C for 40 minutes. The resulting supernatant was loaded onto an amylose column and incubated for 2 h. It was subsequently washed with a buffer composed of 25 mM Hepes, pH 7.5, 150 mM NaCl, 0.01% LMNG, and 0.002% CHS, and then eluted using the same buffer containing 10 mM maltose. After concentration and overnight TEV cleavage at 4 °C, the eluate was separated on a Superdex 200 Increase 10/300 GL (GE Health Science) gel filtration column using a buffer of 25 mM HEPES, pH 7.5, 150 mM NaCl, 0.00075% (w/v) LMNG, 0.00025% glyco-diosgenin (GDN), and 0.0002% (w/v) detergent (Anatrace). The corresponding peak was concentrated to 10 mg/ml and then rapidly frozen for subsequent grid preparation.

TOPFlash assay

The TOPFlash assay was conducted using HEK293T embryonic kidney cells. Cell-based luciferase assays were carried out according to previously established methods[28]. In brief, cells were initially seeded at a density of 20,000 cells per well in a 24-well plate and incubated for 24 h in DMEM (Gibco) supplemented with 5% fetal bovine serum prior to transfection. Subsequently, the cells were transfected with the following components per well: 10 ng of FZD4-eYFP expression plasmid, 10 ng of LRP6 expression plasmid, 100 ng of the Super-TOPFlash TCF-luciferase reporter, 10 ng of the ligand expression vector (WNT3a or Norrin or vehicle), and 1 ng of the phRGtkRenilla control plasmid. Transfections were carried out using X-tremeGene 9 (Roche). Cell collection and lysis were performed 48 h post-transfection. Luminescence activities were assessed using the Dual Luciferase Kit (Promega), following the manufacturer's instructions. Renilla luciferase activity served as a transfection control. All activities were normalized (expressed as relative activities) in comparison to the basal activity of the wild-type FZD, which was set as 1.0.

MBP-Norrin expression and purification

The N-terminal fusion of human Norrin (residues 25–133) with MBP was cloned into the primary cloning site of the pETDuet1 vector from Novagen. This vector also accommodated a Dsbc cDNA in the secondary cloning site. The expression of Norrin was conducted in Escherichia coli Origami B (DE3) strain, following a procedure akin to that detailed in prior work[56], with some minor adjustments. To summarize, the MBP-Norrin protein was subjected to refolding within a solution containing 1 M L-arginine, 20 mM Tris (pH 8.5), 0.5 M NaCl, 1 mM GSH, 1 mM GSSG, and 1 mM EDTA. The resulting active dimeric protein was subsequently purified using a Heparin column (GE Health Science), followed by another purification step with a Superdex 200 Increase 10/300 GL column (GE Health Science). The peak fraction from this purification was concentrated to 2 mg/ml and then flash-frozen for use in subsequent experiments.

BRET assay

In accordance with the published paper[23], the BRET experiments were conducted using a receptor-Nluc plasmid at a concentration of 500 ng/μl and a cp173Venus-DVL2/PDZ-DEP/DEP plasmid at the same concentration of 500 ng/μl. The BRET0 signal was assessed using either a ClarioStar (BMG) or SPARK (Tecan) plate reader, employing band-pass filters set at 535–30 nm (for acceptor) and 475–30 nm (for donor), or a monochromator set within the range of 535 to 560 nm (for acceptor) and 430 to 455 nm (for donor) with an integration time of 100 ms, unless explicitly stated otherwise. Cell seeding was performed in white 96-well plates with flat bottoms (Greiner BioOne), pre-coated with PDL. Twenty-two hours post-transfection, the cells were washed once with 200 μl of HBSS (Hanks' Balanced Salt Solution) and maintained in HBSS. In these experiments, Venus fluorescence was initially quantified. Subsequently, 10 μl of furimazine (Promega), achieving a final dilution of 1:1000, were added to reach a final volume of 90 μl. After a 5-minute incubation following this addition, luminescence was recorded three times. Following that, 10 μl of the ligand were added to attain a final volume of 100 μl, and luminescence measurements were continued for 30 readings, extending over a period of 45 minutes. All measurements were carried out at a temperature of 37 °C using a PerkinElmer EnVision Multilabel Plate Reader.

Western-blot

For receptor, AD293 cells were subjected to transfection with 100 ng of pcDNA3-FZD4-eYFP per well in a 24-well plate, employing PEI at a 1:5 ratio. After a 48-h incubation post-transfection, the cells were lysed using Cell Lysis Reagent from Sigma. The cellular lysates' proteins were subsequently separated on a 10% Bis-Tris gel at a voltage of 170 V for 1 h, followed by a transfer onto a polyvinylidene difluoride (PVDF) membrane at 100 V for 1.5 h. The membranes were blocked with 10% milk dissolved in TBS-T (20 mM Tris-HCl, pH 7.5, 50 mM NaCl, 0.1% Tween-20) for a duration of 30 minutes at room temperature. One of the membranes was exposed to mouse anti-GFP-Tag monoclonal antibody (1:5000, ABclonal) in TBS-T over 2 h at room temperature. Meanwhile, another membrane was treated with β-actin mouse monoclonal antibody (1:10,000, ABclonal) in TBS-T containing 3% milk, also for a duration of 2 h at room temperature. Subsequently, the membranes were subjected to TBS-T rinses and incubated with

HRP-conjugated goat anti-mouse IgG (1:5000, ABclonal) for 30 minutes in TBS-T. The protein bands were detected using the iBright CL1000 imaging system (Thermo Fisher Scientific) following treatment with a chemiluminescent substrate (Thermo Fisher Scientific). As DVL2, AD293 cells were transfected with 100 ng of pcDNA3-DVL2/PDZ-DEP/DEP-3flag. One of the membranes was treated with monoclonal anti-FLAG M2 peroxidase (HRP) antibody (1:5000, Sigma) in TBS-T for 2 h at room temperature. The subsequent steps remained consistent with those mentioned above.

Grid preparation and cryo-EM data collection

A protein complex sample of 3–5 μl with a concentration of approximately 10 mg/ml was applied to glow-charged Quantifoil R1.2/1.3 Cu holey carbon grids (Quantifoil GmbH). These grids were subsequently plunge-frozen in liquid ethane using a Vitrobot Mark IV instrument from Thermo Fisher Scientific. The settings used were a blot force of 10, a blot time of 5 seconds, a humidity level of 100%, and a temperature of 4 °C. The prepared grids, which contained particles evenly distributed in a thin layer of ice, were then loaded into a FEI 300 kV Titan Krios transmission electron microscope, equipped with a Gatan Quantum energy filter. Imaging was carried out using a Gatan K2 Summit direct electron detector with super-resolution counting mode, with a pixel size of 0.55 Å at a magnification of 64,000×. The energy filter slit was set to 20 eV. Each image was composed of 40 frames, resulting in a total exposure time of 7.3 seconds, with a dose rate of 1.5 electrons per square angstrom per second (total dose 60 e/Å^2). The nominal defocus value ranged from −1.2 to −2.2 μm.

Data processing

A total of 3632 raw movie frames were initially subjected to one round of binning (1.1 Å per pixel) and underwent motion correction using MotionCor2[57]. Subsequently, the parameters for the contrast transfer function (CTF) were determined using CTFFIND 4.1[58]. Particle selection was carried out using crYOLO[59], followed by two rounds of reference-free 2D classification within RELION[60]. The well-defined 2D features obtained from this classification were then utilized to create initial models through cryoSPARC's ab initio method[61]. These generated initial models, comprising both good and bad references, were employed for two rounds of hetero-refinement. Following this, the particles were transferred to RELION for 3D classification, without alignment, while applying a mask to isolate the complex. The best class resulting from this classification was subsequently transferred back to cryoSPARC for Non-uniform refinement, which was followed by Bayesian polishing[62] and additional rounds of Non-uniform refinement, ultimately yielding a map with a resolution of 3.53 Å. For the final local refinement in cryoSPARC, a mask was created specifically for ProtA. The resolution of the map was estimated using the gold standard Fourier Shell Correlation (FSC) criterion at FSC = 0.143, and local resolution assessments were carried out using an integrated program within cryoSPARC.

Model building

We initiated the process of model reconstruction against the electron microscopy map by utilizing the AlphaFold prediction[63] for human FZD4 (AF-Q9ULV1-v1) and the NMR structure of DEP (PDB:1fsh)[22] as our starting models. We employed UCSF Chimera[64] to dock these models within the density map. Subsequent to this, we carried out a series of iterative manual refinements in Coot[65] to enhance the precision and quality of the models. Additionally, we utilized Rosetta cryoEM refinement[66] and Phenix real space refinement[67] to further improve the structural accuracy. For the purposes of visualizing and preparing structural figures, we relied on UCSF ChimeraX[68] and PyMOL (accessible at https://pymol.org/2/).

NanoBiT membrane recruitment assay

The N-terminally SmBiT-fused DVL2 was expressed with the plasma membrane-localizing LgBiT construct (LgBiT-CAAX). AD293 cells cultured in the 6-cm culture dish were transfected with a plasmid mixture consisting of 200 ng pcDNA3.1-FZD4, pcDNA3.1-DVL2-SmBiT and PCAGGS-LgBiT-CAAX. The transfected cells were dispensed in a 96-well plate with flat bottoms, add 20 ul of 50 uM CTZ to each cell, RT (about 25 C) for 2 h, in darkness. Then uses US Lumi to measure. All measurements were carried out at room temperature (~25 °C) using a PerkinElmer EnVision Multilabel Plate Reader.

Confocal

FZD4 and FZD4-I416A were fused with RFP, while the DVL2 was fused with GFP, then 300 ng FZD4-RFP or FZD4-I416A- RFP were transfected with 300 ng DVL2- GFP into HeLa by lifpofectamine 2000 at ratio of 1:2 for around 20 h. Single confocal images were acquired at identical settings with 100× oil immersion lens of Zeiss Confocal Microscope LSM880 with fast airyscan.

Reporting summary

Further information on research design is available in the Nature Portfolio Reporting Summary linked to this article.

Data availability

All data produced or analyzed in this study are included in the main text or the supplementary materials. The cryo-EM density maps and atomic coordinates have been deposited in the Electron Microscopy Data Bank (EMDB) and Protein Data Bank (PDB) under accession numbers EMD-37646 and 8WM9 for the FZD4/DEP dimeric complex, and EMD-37647 and 8WMA for the local refined FZD4/DEP protomer A complex. Source data are provided with this paper.

References

1. Clevers, H. Wnt/beta-catenin signaling in development and disease. *Cell* **127**, 469–480 (2006).
2. Perugorria, M. J. et al. Wnt-β-catenin signalling in liver development, health and disease. *Nat. Rev. Gastroenterol. Hepatol.* **16**, 121–136 (2019).
3. Logan, C. Y. & Nusse, R. The Wnt signaling pathway in development and disease. *Annu Rev. Cell Dev. Bi* **20**, 781–810 (2004).
4. Clevers, H. & Nusse, R. Wnt/β-catenin signaling and disease. *Cell* **149**, 1192–1205 (2012).
5. MacDonald, B. T., Tamai, K. & He, X. Wnt/beta-catenin signaling: components, mechanisms, and diseases. *Dev. Cell* **17**, 9–26 (2009).
6. Liu, J. et al. Wnt/β-catenin signalling: function, biological mechanisms, and therapeutic opportunities. *Signal Transduct. Target Ther.* **7**, 3 (2022).
7. Niehrs, C. The complex world of WNT receptor signalling. *Nat. Rev. Mol. Cell Biol.* **13**, 767–779 (2012).
8. Schulte, G. International union of basic and clinical pharmacology. LXXX. The class frizzled receptors. *Pharmacol. Rev.* **62**, 632–667 (2010).
9. Katanaev, V. & Buestorf, S. Frizzled Proteins are bona fide G Protein-Coupled Receptors. *Nat. Prec.* https://doi.org/10.1038/npre.2009.2765.1 (2009).
10. Wright, S. C. et al. A conserved molecular switch in Class F receptors regulates receptor activation and pathway selection. *Nat. Commun.* **10**, 667 (2019).
11. Riobo, N. A., Saucy, B., Dilizio, C. & Manning, D. R. Activation of heterotrimeric G proteins by Smoothened. *Proc. Natl Acad. Sci. USA* **103**, 12607–12612 (2006).
12. Wang, Y. et al. Norrin/Frizzled4 signaling in retinal vascular development and blood brain barrier plasticity. *Cell* **151**, 1332–1344 (2012).

13. Bang, I. et al. Biophysical and functional characterization of Norrin signaling through Frizzled4. *Proc. Natl Acad. Sci. USA* **115**, 8787–8792 (2018).
14. DeBruine, Z. J., Xu, H. E. & Melcher, K. Assembly and architecture of the Wnt/β-catenin signalosome at the membrane. *Br. J. Pharm.* **174**, 4564–4574 (2017).
15. Shen, G. et al. Structural basis of the Norrin-Frizzled 4 interaction. *Cell Res* **25**, 1078–1081 (2015).
16. Chang, T. H. et al. Structure and functional properties of Norrin mimic Wnt for signalling with Frizzled4, Lrp5/6, and proteoglycan. *eLife* https://doi.org/10.7554/eLife.06554 (2015).
17. Petersen, J. et al. Agonist-induced dimer dissociation as a macromolecular step in G protein-coupled receptor signaling. *Nat. Commun.* **8**, 226 (2017).
18. Sharma, M., Castro-Piedras, I., Simmons, G. E. Jr. & Pruitt, K. Dishevelled: A masterful conductor of complex Wnt signals. *Cell Signal* **47**, 52–64 (2018).
19. Wong, H. C. et al. Direct binding of the PDZ domain of Dishevelled to a conserved internal sequence in the C-terminal region of Frizzled. *Mol. Cell* **12**, 1251–1260 (2003).
20. Umbhauer, M. et al. The C-terminal cytoplasmic Lys-thr-X-X-X-Trp motif in frizzled receptors mediates Wnt/beta-catenin signalling. *EMBO J.* **19**, 4944–4954 (2000).
21. Gammons, M. V., Rutherford, T. J., Steinhart, Z., Angers, S. & Bienz, M. Essential role of the Dishevelled DEP domain in a Wnt-dependent human-cell-based complementation assay. *J. Cell Sci.* **129**, 3892–3902 (2016).
22. Wong, H. C. et al. Structural basis of the recognition of the dishevelled DEP domain in the Wnt signaling pathway. *Nat. Struct. Biol.* **7**, 1178–1184 (2000).
23. Bowin, C. F. et al. WNT stimulation induces dynamic conformational changes in the Frizzled-Dishevelled interaction. *Sci. Signal* **16**, eabo4974 (2023).
24. Mahoney, J. P. et al. PI(4,5)P(2)-stimulated positive feedback drives the recruitment of Dishevelled to Frizzled in Wnt-β-catenin signaling. *Sci. Signal* **15**, eabo2820 (2022).
25. Kang, K., Shi, Q., Wang, X. & Chen, Y. G. Dishevelled phase separation promotes Wnt signalosome assembly and destruction complex disassembly. *J. Cell Biol.* https://doi.org/10.1083/jcb.202205069 (2022).
26. Alshahrani, S. H. et al. Dishevelled: An emerging therapeutic oncogene in human cancers. *Pathol. Res Pr.* **250**, 154793 (2023).
27. Janda, C. Y., Waghray, D., Levin, A. M., Thomas, C. & Garcia, K. C. Structural basis of Wnt recognition by Frizzled. *Science* **337**, 59–64 (2012).
28. Yang, S. et al. Crystal structure of the Frizzled 4 receptor in a ligand-free state. *Nature* **560**, 666–670 (2018).
29. Beaumont, K. A. et al. Receptor function, dominant negative activity and phenotype correlations for MC1R variant alleles. *Hum. Mol. Genet* **16**, 2249–2260 (2007).
30. Zhu, X. G., Yu, C. L., McPhie, P., Wong, R. & Cheng, S. Y. Understanding the molecular mechanism of dominant negative action of mutant thyroid hormone beta 1-receptors: the important role of the wild-type/mutant receptor heterodimer. *Endocrinology* **137**, 712–721 (1996).
31. Yudt, M. R., Jewell, C. M., Bienstock, R. J. & Cidlowski, J. A. Molecular origins for the dominant negative function of human glucocorticoid receptor beta. *Mol. Cell Biol.* **23**, 4319–4330 (2003).
32. Yao, X. J. et al. The effect of ligand efficacy on the formation and stability of a GPCR-G protein complex. *Proc. Natl Acad. Sci. USA* **106**, 9501–9506 (2009).
33. Gregorio, G. G. et al. Single-molecule analysis of ligand efficacy in β(2)AR-G-protein activation. *Nature* **547**, 68–73 (2017).
34. Duan, J. et al. Cryo-EM structure of an activated VIP1 receptor-G protein complex revealed by a NanoBiT tethering strategy. *Nat. Commun.* **11**, 4121 (2020).
35. Xia, R. et al. Cryo-EM structure of the human histamine H1 receptor/Gq complex. *Nat. Commun.* **12**, 2086 (2021).
36. Wang, N. et al. Structural basis of leukotriene B4 receptor 1 activation. *Nat. Commun.* **13**, 1156 (2022).
37. Qian, Y. et al. Structural insights into adhesion GPCR ADGRL3 activation and G(q), G(s), G(i), and G(12) coupling. *Mol. Cell* **82**, 4340–4352.e4346 (2022).
38. Xu, W. et al. Structural basis for strychnine activation of human bitter taste receptor TAS2R46. *Science* **377**, 1298–1304 (2022).
39. Guo, L. et al. Structural basis of amine odorant perception by a mammal olfactory receptor. *Nature* **618**, 193–200 (2023).
40. Xu, P. et al. Structural insights into the lipid and ligand regulation of serotonin receptors. *Nature* **592**, 469–473 (2021).
41. Isberg, V. et al. Generic GPCR residue numbers - aligning topology maps while minding the gaps. *Trends Pharm. Sci.* **36**, 22–31 (2015).
42. Penton, A., Wodarz, A. & Nusse, R. A mutational analysis of dishevelled in Drosophila defines novel domains in the dishevelled protein as well as novel suppressing alleles of axin. *Genetics* **161**, 747–762 (2002).
43. Rasmussen, S. G. et al. Crystal structure of the beta2 adrenergic receptor-Gs protein complex. *Nature* **477**, 549–555 (2011).
44. Qi, X. et al. Cryo-EM structure of oxysterol-bound human Smoothened coupled to a heterotrimeric G(i). *Nature* **571**, 279–283 (2019).
45. Zhu, X. et al. Structural basis of adhesion GPCR GPR110 activation by stalk peptide and G-proteins coupling. *Nat. Commun.* **13**, 5513 (2022).
46. Xu, L. et al. Cryo-EM structure of constitutively active human Frizzled 7 in complex with heterotrimeric G(s). *Cell Res* **31**, 1311–1314 (2021).
47. Wess, J. Molecular basis of receptor/G-protein-coupling selectivity. *Pharm. Ther.* **80**, 231–264 (1998).
48. Lee, Y. et al. Molecular basis of β-arrestin coupling to formoterol-bound β(1)-adrenoceptor. *Nature* **583**, 862–866 (2020).
49. Duan, J. et al. GPCR activation and GRK2 assembly by a biased intracellular agonist. *Nature* **620**, 676–681 (2023).
50. Wang, C. et al. Structure of the human smoothened receptor bound to an antitumour agent. *Nature* **497**, 338–343 (2013).
51. Yue, Y. et al. Structural insight into apelin receptor-G protein stoichiometry. *Nat. Struct. Mol. Biol.* **29**, 688–697 (2022).
52. Papasergi-Scott, M. M. et al. Structures of metabotropic GABA(B) receptor. *Nature* **584**, 310–314 (2020).
53. Gammons, M. V., Renko, M., Johnson, C. M., Rutherford, T. J. & Bienz, M. Wnt Signalosome Assembly by DEP Domain Swapping of Dishevelled. *Mol. Cell* **64**, 92–104 (2016).
54. Seven, A. B. et al. G-protein activation by a metabotropic glutamate receptor. *Nature* **595**, 450–454 (2021).
55. Tauriello, D. V. et al. Wnt/β-catenin signaling requires interaction of the Dishevelled DEP domain and C terminus with a discontinuous motif in Frizzled. *Proc. Natl Acad. Sci. USA* **109**, E812–E820 (2012).
56. Ke, J. et al. Structure and function of Norrin in assembly and activation of a Frizzled 4-Lrp5/6 complex. *Genes Dev.* **27**, 2305–2319 (2013).
57. Zheng, S. Q. et al. MotionCor2: anisotropic correction of beam-induced motion for improved cryo-electron microscopy. *Nat. methods* **14**, 331–332 (2017).
58. Rohou, A. & Grigorieff, N. CTFFIND4: Fast and accurate defocus estimation from electron micrographs. *J. Struct. Biol.* **192**, 216–221 (2015).
59. Wagner, T. et al. SPHIRE-crYOLO is a fast and accurate fully automated particle picker for cryo-EM. *Commun. Biol.* **2**, 218 (2019).

60. Zivanov, J. *et al*. New tools for automated high-resolution cryo-EM structure determination in RELION-3. *eLife* https://doi.org/10.7554/eLife.42166 (2018).
61. Punjani, A., Rubinstein, J. L., Fleet, D. J. & Brubaker, M. A. cryoSPARC: algorithms for rapid unsupervised cryo-EM structure determination. *Nat. methods* **14**, 290–296 (2017).
62. Zivanov, J., Nakane, T. & Scheres, S. H. W. A Bayesian approach to beam-induced motion correction in cryo-EM single-particle analysis. *IUCrJ* **6**, 5–17 (2019).
63. Jumper, J. et al. Highly accurate protein structure prediction with AlphaFold. *Nature* **596**, 583–589 (2021).
64. Pettersen, E. F. et al. UCSF Chimera–a visualization system for exploratory research and analysis. *J. Comput Chem.* **25**, 1605–1612 (2004).
65. Emsley, P. & Cowtan, K. Coot: model-building tools for molecular graphics. *Acta Crystallogr. D. Biol. Crystallogr* **60**, 2126–2132 (2004).
66. Wang, R. Y. et al. Automated structure refinement of macromolecular assemblies from cryo-EM maps using Rosetta. *eLife* https://doi.org/10.7554/eLife.17219 (2016).
67. Adams, P. D. et al. PHENIX: a comprehensive Python-based system for macromolecular structure solution. *Acta Crystallogr. D. Biol. Crystallogr* **66**, 213–221 (2010).
68. Pettersen, E. F. et al. UCSF ChimeraX: Structure visualization for researchers, educators, and developers. *Protein Sci.: Publ. Protein Soc.* **30**, 70–82 (2021).

Acknowledgements

This work was supported by the Startup Funds of HIT Center for Life Sciences; the National Natural Science Foundation of China (32070048 to Y.H., 32071194 to F.X.). We thank Dr. Jijie Chai of Westlake University for his comments and suggestions on the manuscript. We thank Prof. Ye-Guang Chen of Tsinghua University for the gift of DVL1/2/3 TKO HEK293T cells.

Author contributions

Y.Q. made the expression constructs, expressed and purified the proteins, prepared and screened grids, made mutations, performed functional assays, prepared the figures and analyzed data. Z.M. expressed and purified the proteins, made mutations, performed functional assays and analyzed data. Z.X. and Y.X. made mutations and performed functional assay. Y.D. contributed methodology. R.X., X.Z., Z.Z., X.T., H.Y., J.L., J.S. and Y.L. prepared plasmids, cultured cells and prepared reagent. A.Z. and C.G. collected the cryo-EM data. J.K. contributed to the methodology of Norrin Purification. L.J. and W.J.K. searched drosophila database and identified *dsh* DEP mutants. F.X. and Z.H. analyzed data and edited the manuscript. Y.H. conceived the project, designed the experiments, analyzed data, solved the structure and wrote the manuscript and supervised the project. All authors contributed to data interpretation and preparation of the manuscript.

Competing interests

The authors declare no competing interests.

Additional information

Supplementary information The online version contains supplementary material available at https://doi.org/10.1038/s41467-024-52174-z.

Correspondence and requests for materials should be addressed to Yuanzheng He.

Peer review information *Nature Communications* thanks Gary Davidson, and the other, anonymous, reviewer(s) for their contribution to the peer review of this work. A peer review file is available.